zjv-jvi/zjv00518/zjv3323d18z | xppws | S=3 | 12/16/17 | 5:49 | 4/Color Fig: 2,4,5,6,9,10 | ArtID: 01727-17 | DOI:10.1128/JVI.01727-17 | CE: ysf

Editor: Simon | Section: Genetic Diversity and Evolution | Designation: T

AMERICAN SOCIETY FOR MICROBIOLOGY | Journal of Virology®

GENETIC DIVERSITY AND EVOLUTION

Novel *Sulfolobus* Virus with an Exceptional Capsid Architecture

AQ: au

Haina Wang,[a] Zhenqian Guo,[b] Hongli Feng,[b] Yufei Chen,[c] Xiuqiang Chen,[a] Zhimeng Li,[a] Walter Hernández-Ascencio,[d] Xin Dai,[a,f] Zhenfeng Zhang,[a] Xiaowei Zheng,[a] Marielos Mora-López,[d] Yu Fu,[a] Chuanlun Zhang,[e] Ping Zhu,[b,f] Li Huang[a,f]

[a]State Key Laboratory of Microbial Resources, Institute of Microbiology, Chinese Academy of Sciences, Beijing, China

[b]National Laboratory of Biomacromolecules, CAS Center for Excellence in Biomacromolecules, Institute of Biophysics, Chinese Academy of Sciences, Beijing, China

[c]State Key Laboratory of Marine Geology, Tongji University, Shanghai, China

AQ:A [d]Centro de Biología Celular y Molecular, Universidad de Costa Rica, San Pedro de Montes de Oca, Costa Rica

[e]Department of Ocean Science and Engineering, South University of Science and Technology, Shenzhen, China

[f]College of Life Sciences, University of Chinese Academy of Sciences, Beijing, China

ABSTRACT A novel archaeal virus, denoted *Sulfolobus ellipsoid virus 1* (SEV1), was isolated from an acidic hot spring in Costa Rica. The morphologically unique virion of SEV1 contains a protein capsid with 16 regularly spaced striations and an 11-nm-thick envelope. The capsid exhibits an unusual architecture in which the viral DNA, probably in the form of a nucleoprotein filament, wraps around the longitudinal axis of the virion in a plane to form a multilayered disk-like structure with a central hole, and 16 of these structures are stacked to generate a spool-like capsid. SEV1 harbors a linear double-stranded DNA genome of ~23 kb, which encodes 38 predicted open reading frames (ORFs). Among the few ORFs with a putative function is a gene encoding a protein-primed DNA polymerase. Sixfold symmetrical virus-associated pyramids (VAPs) appear on the surface of the SEV1-infected cells, which are ruptured to allow the formation of a hexagonal opening and subsequent release of the progeny virus particles. Notably, the SEV1 virions acquire the lipid membrane in the cytoplasm of the host cell. The lipid composition of the viral envelope correlates with that of the cell membrane. These results suggest the use of a unique mechanism by SEV1 in membrane biogenesis.

IMPORTANCE Investigation of archaeal viruses has greatly expanded our knowledge of the virosphere and its role in the evolution of life. Here we show that *Sulfolobus ellipsoid virus 1* (SEV1), an archaeal virus isolated from a hot spring in Costa Rica, exhibits a novel viral shape and an unusual capsid architecture. The SEV1 DNA wraps multiple times in a plane around the longitudinal axis of the virion to form a disk-like structure, and 16 of these structures are stacked to generate a spool-like capsid. The virus acquires its envelope intracellularly and exits the host cell by creating a hexagonal hole on the host cell surface. These results shed significant light on the diversity of viral morphogenesis.

KEYWORDS archaeal virus, capsid architecture, membrane acquisition, virion assembly, virus release

The past 2 decades have witnessed the rapid expansion in our knowledge of the diversity of viruses on Earth, in part due to the discovery of a large number of unique viruses infecting crenarchaea (1, 2). Although archaeal viruses account for only ~2% of the total virus tally, they not only show nearly all of the morphotypes known for viruses infecting bacteria and eukaryotes but also exhibit unique and remarkably diverse morphologies never seen before (3, 4). Archaeal viruses have been found to

Received 2 October 2017 **Accepted** 22 November 2017

Accepted manuscript posted online 6 December 2017

Citation Wang H, Guo Z, Feng H, Chen Y, Chen X, Li Z, Hernández-Ascencio W, Dai X, Zhang Z, Zheng X, Mora-López M, Fu Y, Zhang C, Zhu P, Huang L. 2018. Novel *Sulfolobus* virus with an exceptional capsid architecture. J Virol 92:e01727-17. https://doi.org/10.1128/JVI.01727-17.

Editor Anne E. Simon, University of Maryland, College Park

Address correspondence to Ping Zhu, zhup@ibp.ac.cn, or Li Huang, huangl@sun.im.ac.cn.

H.W. and Z.G. contributed equally to this work.

zjv-jvi/zjv00518/zjv3323d18z | xppws | S=3 | 12/16/17 | 5:49 | 4/Color Fig: 2,4,5,6,9,10 | ArtID: 01727-17 | DOI:10.1128/JVI.01727-17 | CE: ysf

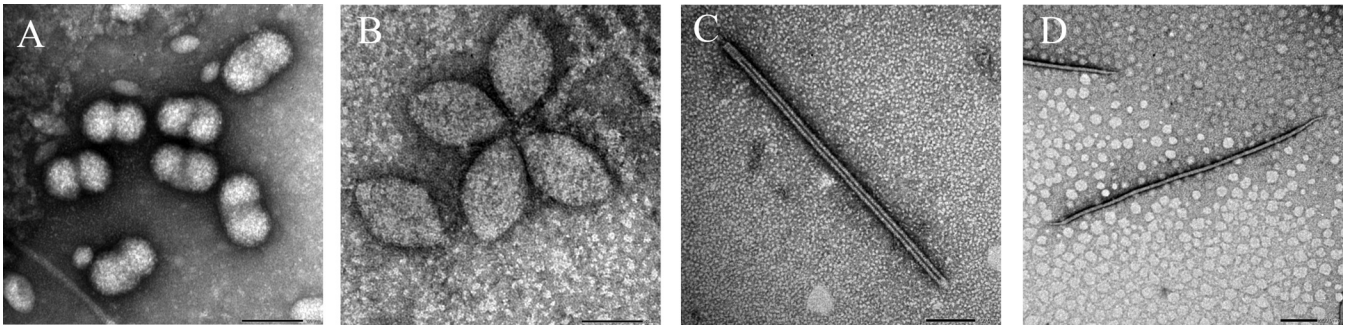

FIG 1 Various virus-like particles from an acidic hot spring in Costa Rica. An enrichment culture was developed with an acidic hot spring sample from Costa Rica. The cell-free supernatant was stained with uranyl acetate and examined by electron microscopy. (A) Ellipsoid particles; (B) spindle-shaped particles; (C) a rod-like particle; (D) a filamentous particle. Bars, 100 nm (A), 50 nm (B), 100 nm (C), 200 nm (D).

occur in unusual shapes such as a spindle, a bottle, and a droplet, in addition to more-common shapes such as a head-tail structure, a sphere, a rod, and a filament. The majority of archaeal viral genes encode an unknown function, suggesting that archaeal viruses hold a huge gene pool for the evolution of life in general and *Archaea* in particular. Therefore, investigation of archaeal viruses will provide clues to the origin and evolution of various cellular processes.

Archaeal viruses are known to employ various strategies in packaging their genomes and releasing their progeny virions from the host cells (5). Some archaeal viral genomes are packaged within a protein shell or a capsid of different shapes. These include tailless icosahedral viruses of the families *Turriviridae* and *Sphaerolipoviridae* (6, 7), filamentous viruses of the *Tristromaviridae* (8), and spindle-shaped viruses of the *Fuselloviridae* (9). Other archaeal viral genomes are not encased in a protein shell but instead are condensed by capsid proteins into various architectural forms, such as a cylinder (e.g., filamentous viruses of the order *Ligamenvirales*) (10, 11), a sphere (e.g., spherical viruses of the *Globuloviridae* and *Portogloboviridae*) (12, 13), a cone (e.g., bottle-shaped viruses of the *Ampullaviridae*) (14), and a coil (e.g., spiral coil-like viruses of the *Spiraviridae*) (15). Moreover, archaeal viruses are either enveloped or naked. The egress mechanisms of archaeal viruses are also diverse. Virions of the fusellovirus *Sulfolobus spindle-shaped virus 1* (SSV1) bud from the host cell, acquiring its envelope during the budding process (16). Although morphologically different, mature virions of the *Rudiviridae* and *Turriviridae* exit the host cell through a 7-fold symmetrical structure, known as the virus-associated pyramid (VAP) on the cell surface (17, 18). In addition, 6-fold symmetrical VAPs have been observed on the surface of *Pyrobaculum oguniense*, although viral replication has yet to be demonstrated (19). Release of mature virions of the family *Tristromaviridae* and of the archaeal members of the order *Caudovirales* occurs by cell lysis (8).

In this article, we describe a novel archaeal virus isolated from a hot spring in Costa Rica. The virus, named *Sulfolobus ellipsoid virus 1* (SEV1), exhibits an ellipsoid morphology and a spool-like capsid architecture. The virus acquires its envelope intracellularly and exits the host cell by rupturing 6-fold symmetrical VAPs on the cell surface.

RESULTS

Identification of SEV1 and its host. A sediment sample was collected from an acidic hot spring (86 to 106°C, pH 2.2 to 2.5) in Lagura Fumarolica, Costa Rica, and used to establish an enrichment culture in Zillig's medium (20). At least four types of virus-like particles (VLPs), in the shapes of a peanut, a spindle, a filament, and a rod, were observed under transmission electron microscope (TEM) in the supernatant of the enrichment culture (Fig. 1). While the last three morphologies were often found among *Sulfolobus* viruses, the peanut shape appeared quite unusual. To learn more about the peanut-shaped VLP, we first obtained a virus-free strain, a potential host for the virus, from the enrichment culture by picking single colonies containing VLPs including the

zjv-jvi/zjv00518/zjv3323d18z | xppws | S=3 | 12/16/17 | 5:49 | 4/Color Fig: 2,4,5,6,9,10 | ArtID: 01727-17 | DOI:10.1128/JVI.01727-17 | CE: ysf

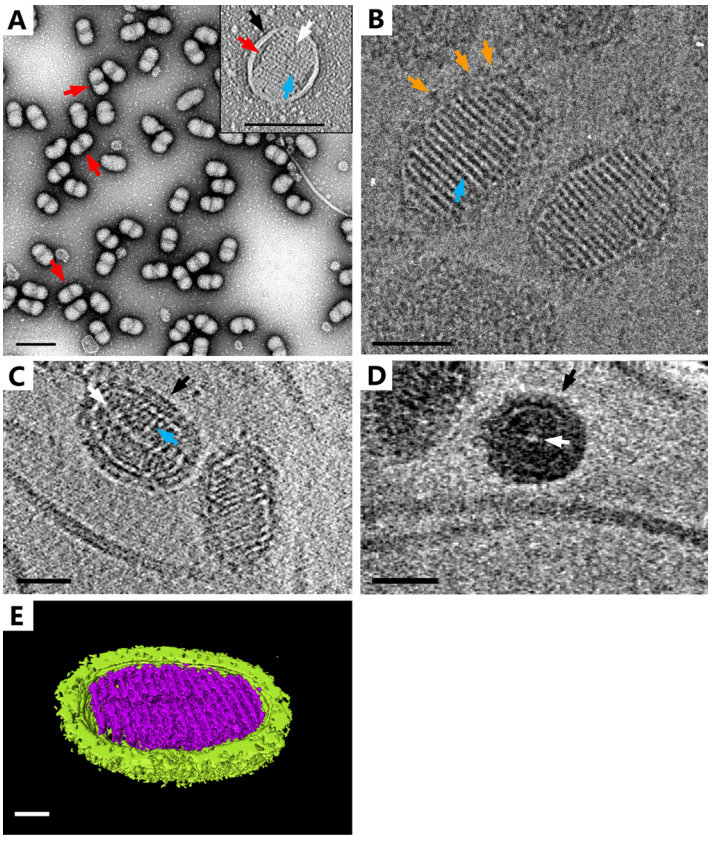

COLOR

FIG 2 Morphology of the SEV1 virion. (A) Electron micrographs of SEV1 virions negatively stained with 2% uranyl acetate. The virions are slightly constricted in the middle, as indicated by red arrows. Bar, 200 nm. Inset, an SEV1 virion. The envelope, capsid striations, and central hole of the virion are indicated by black, blue, and white arrows, respectively. Bar, 100 nm. (B) Cryo-ET of SEV1 virions. The spikes on the virus envelope and striated capsid are indicated by orange and blue arrows, respectively. Bar, 50 nm. (C) A thin slice (~16.12 Å) from the cryo-ET of SEV1. The central hole in the capsid is indicated by a white arrow. The envelope and striated capsid are indicated by black and blue arrows, respectively. Bar, 50 nm. (D) A sectioned slice from the reconstructed tomogram of an SEV1 virion (top view). Bar, 50 nm. The envelope and central hole are indicated by black and white arrows, respectively. (E) A 3-D surface rendering model of the reconstructed SEV1 virion as shown in panel C. The SEV1 virion is surrounded by a lipid membrane decorated with spikes (yellow), and the interior of the SEV1 virion is striated (purple). Bar, 20 nm.

AQ: F

peanut-shaped particles and repeated subculturing in liquid Zillig's medium (see Materials and Methods). This strain was shown to be a novel *Sulfolobus* species, denoted *Sulfolobus* sp. A20 (21). We were then able to purify the peanut-shaped VLPs by infecting *Sulfolobus* sp. A20 with the supernatant of the enrichment culture and picking single colonies. We term this VLP *Sulfolobus ellipsoid virus 1* (SEV1).

Virion morphology and structure. The SEV1 virion is ellipsoidal, measures about 115 nm by 78 nm, and is coated with an envelope (Fig. 2). A slight constriction was observed in the middle of the virion under TEM when the virus particles were negatively stained (Fig. 2A), but no apparent constriction was found under cryo-electron microscope (cryo-EM) (Fig. 2B and C). As revealed by three-dimensional (3-D) electron tomography (ET), there are spaces between the capsid and the envelope, especially in the middle of the virion (inset in Fig. 2A; see also Movie S1 in the supplemental material). Therefore, the observed constriction in the negatively stained samples under TEM may have resulted from the dehydration of the virions on the grids during sample preparation.

F2

As observed under cryo-EM, the SEV1 virion contains a striated capsid enclosed by an 11-nm-thick envelope decorated with protruding spikes (Fig. 2B). Sixteen helical striations aligned perpendicular to the longitudinal axis of the particle with a periodicity

zjv-jvi/zjv00518/zjv3323d18z | xppws | S=3 | 12/16/17 | 5:49 | 4/Color Fig: 2,4,5,6,9,10 | ArtID: 01727-17 | DOI:10.1128/JVI.01727-17 | CE: ysf

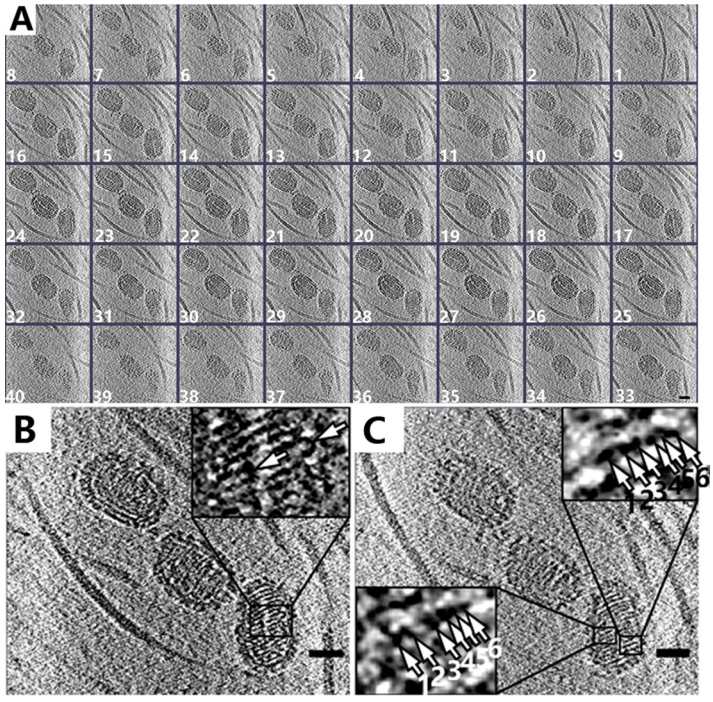

FIG 3 Cryo-electron micrographs of SEV1 virions. (A) Sequential thin slices (~16.14 Å) of a cryo-electron tomogram of SEV1 virions. Numbers indicate the sequence of thin slices. (B) A blow-up view of slice 20 in panel A. Arrows indicate where the nucleoprotein filament goes from one disk to the next. (C) A blow-up view of slice 15 in panel A. Dots, as indicated by numbered arrows, suggest that the nucleoprotein filament wraps around the central axis of the virion six times in a single disk. Bars, 50 nm.

of ~5 nm are clearly visible on the capsid (Fig. 2B and C). Each electron-dense stripe is ~2.8 nm wide. The longitudinal section of the 3-D cryo-ET of a virion reveals a tube-like structure of ~8 nm in diameter at the center of the capsid (Fig. 2C and D). As shown in the 2-D sectioned slices from the cryo-ET of the capsid, apparent striations are also evident in the interior of the particle (Fig. 2C and 3). Considering that the size of the filament is close to that of double-stranded DNA (dsDNA), along with the observations that the virion lacks a protein shell, carries no viral DNA in the central channel, and contains copious amounts of the capsid protein (see below), we propose that the SEV1 capsid is formed by coiling of a nucleoprotein filament. As shown in a top view cross-sectioned slice of the ET in Fig. 2D, the filament wraps tightly around the longitudinal axis multiple times in the middle portion of the capsid, in a plane, to form a disk-like structure (Fig. 2D and 3; see also Movie S2 in the supplemental material). Sixteen of the stacked disks constitute the SEV1 capsid (Fig. 2E and Movie S2). A similar capsid architecture is also apparent in the negative-staining ET of the virion (Fig. 2A, inset, and Movie S1). The capsid is somewhat flexible in shape, presumably due to the variability in the diameter of a disk and in the space between disks (Movie S2). The flexibility of the capsid may have contributed to the constriction of the virion in the middle when the virus particle was dehydrated during analysis by negative-stain TEM.

Genomic features. The sequence of the SEV1 genome was determined by digesting the viral DNA with restriction enzymes, cloning the restriction fragments, and sequencing the inserts. Gaps between contigs were filled by PCR, and the terminal sequences were obtained by primer walking (Fig. 4). The virus harbors a linear double-stranded DNA genome of 23,219 bp with a 172-bp inverted terminal repeat (ITR) at each end (Fig. 4A).

The viral genome, which has a GC content of ~33%, contains 38 predicted open reading frames (ORFs) (>50 amino acid residues in length). The majority (27/38) of the ORFs reside on one of the strands (Fig. 5A; see also Table S1 in the supplemental material). Most of the ORFs encode an unknown function. Four genes (i.e., *vp1*, *vp2*, *vp3*,

zjv-jvi/zjv00518/zjv3323d18z | xppws | S=3 | 12/16/17 | 5:49 | 4/Color Fig: 2,4,5,6,9,10 | ArtID: 01727-17 | DOI:10.1128/JVI.01727-17 | CE: ysf

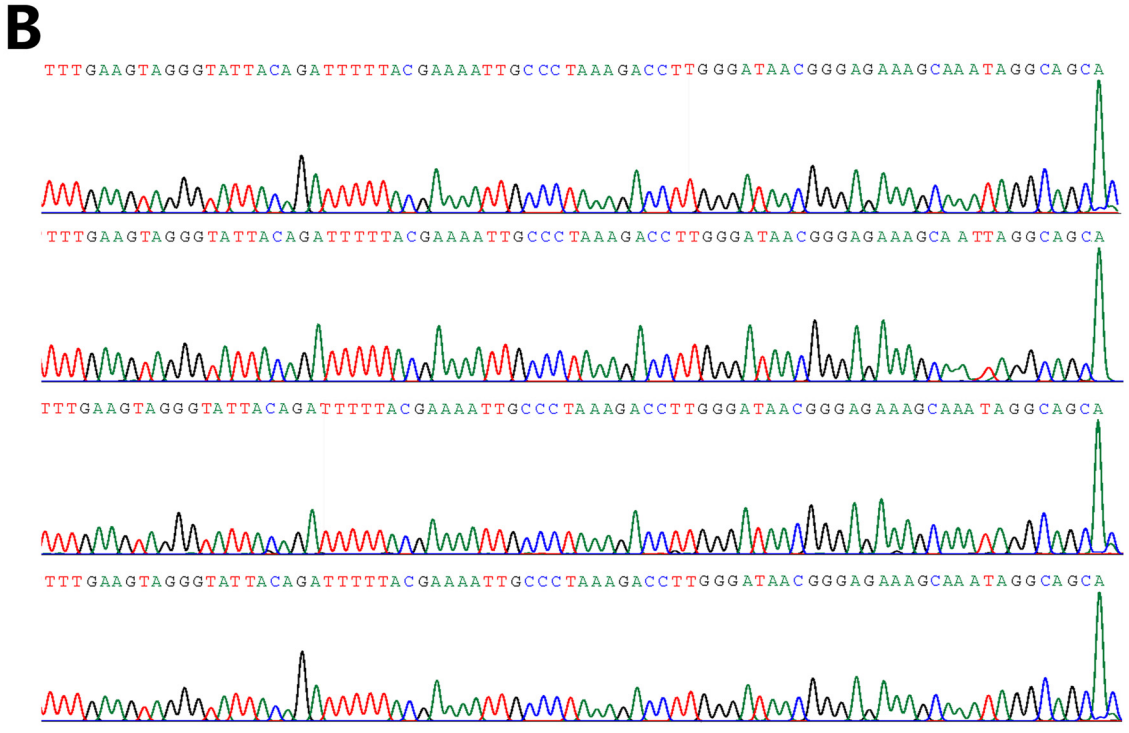

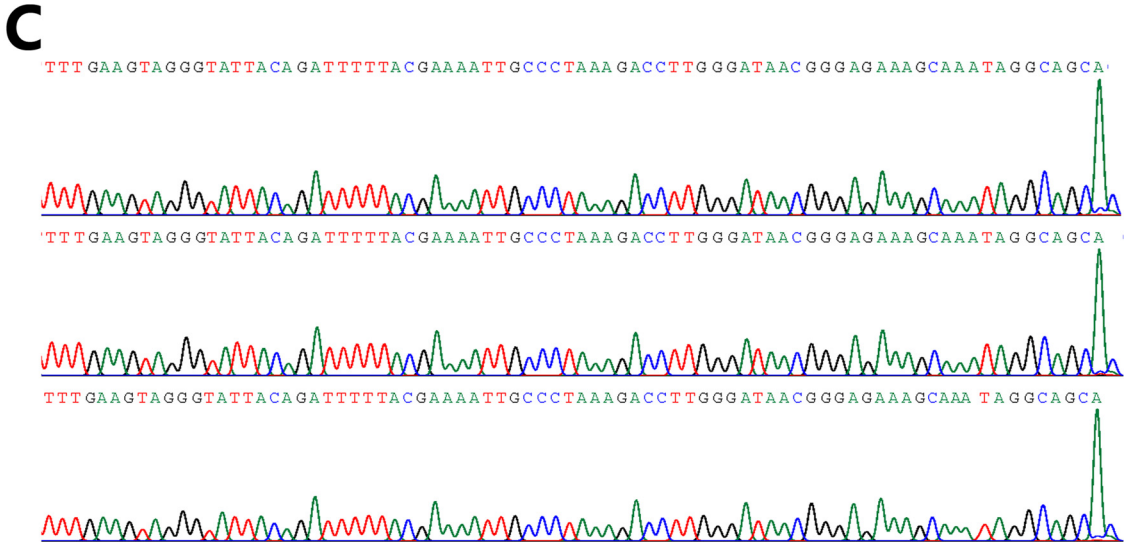

COLOR

FIG 4 Base calling of the terminal regions of the SEV1 genome. (A) Location of primers for primer walking. (B and C) Left (B) and right (C) ends of the SEV1 genome. The large green peak at the end of each trace represents the signal of a nucleotide added to the end of the product of primer extension.

zjv-jvi/zjv00518/zjv3323d18z | xppws | S=3 | 12/16/17 | 5:49 | 4/Color Fig: 2,4,5,6,9,10 | ArtID: 01727-17 | DOI:10.1128/JVI.01727-17 | CE: ysf

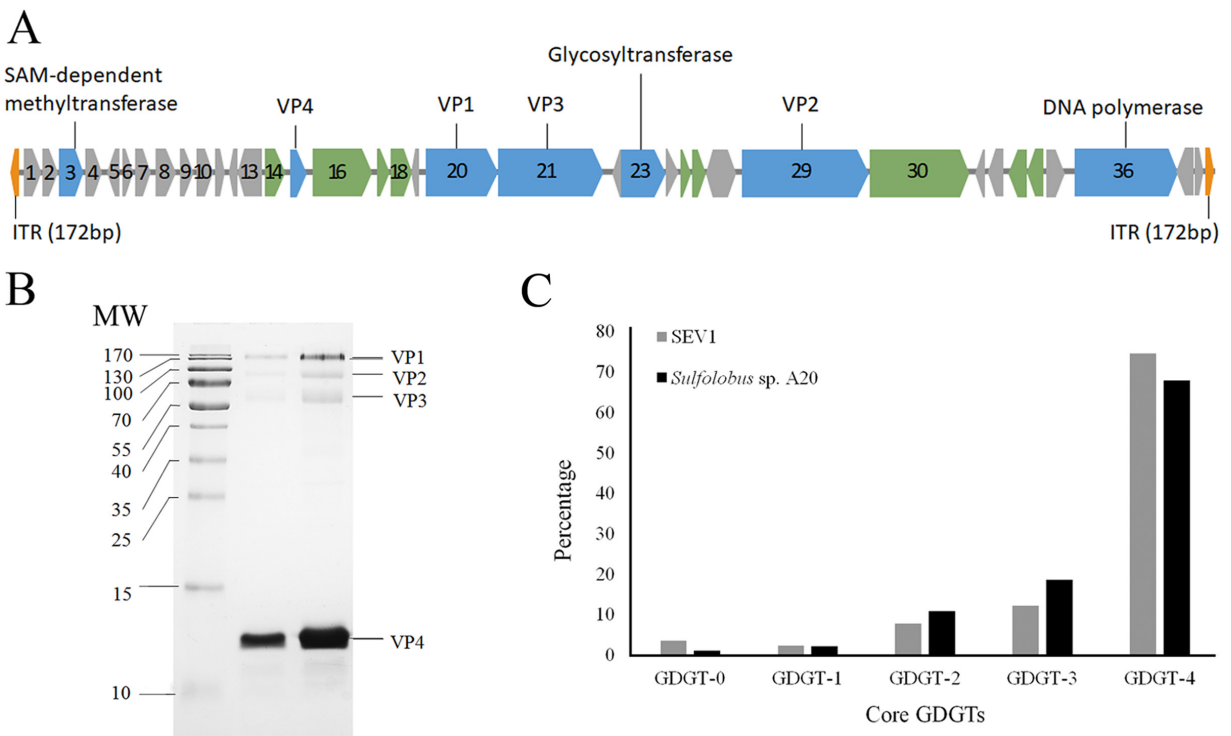

COLOR

FIG 5 Composition of the SEV1 virion. (A) Genome map of SEV1. The size and direction of each predicted ORF or genetic element are indicated by an arrow. ORFs with a putative function, those homologous to ORFs from other archaeal viruses or containing conserved motifs, and those having no significant sequence matches to known sequences in public databases are shown with blue, green, and gray arrows, respectively. The inverted terminal repeats (ITRs) are indicated by orange arrows. (B) SDS-PAGE of the virion proteins of SEV1. Four major structural proteins, denoted VP1, VP2, VP3, and VP4, are shown. Molecular weights (in thousands) of the protein markers are indicated. (C) Relative distributions of GDGTs from SEV1 virions and *Sulfolobus* sp. A20.

and *vp4*) were found to encode the structural proteins of the virus (see below). A BLASTP search of a locally built archaeal viral ORF database revealed seven significant sequence matches (E value, <1e−03) in SEV1 ORFs, i.e., ORF281, ORF665, ORF159, ORF129, ORF381, ORF100, and ORF140 (Table S1). ORF281, ORF665, and ORF159 encode a glycosyltransferase, a B-family DNA polymerase, and an *S*-adenosylmethionine (SAM)-dependent methyltransferase, respectively. The other four ORFs have homologous sequences in lipothrixviruses and/or rudiviruses and, in some cases, in the spindle-shaped virus *Sulfolobus monocaudavirus 1* (SMV1), implying possible horizontal gene transfer between these viruses.

Notably, ORF665 encodes a putative B-type DNA polymerase belonging to the subfamily of protein-primed DNA polymerases, represented by PRD1 and phi29 DNA polymerases (22, 23), since it contains well-conserved DNA polymerase motifs (Pol I, IIa, IIb, and III) in the C-terminal region and less well conserved 3′ to 5′ exonuclease motifs in the N-terminal region, in addition to the signature sequences of protein-primed DNA polymerases, i.e., TPR-1, TPR-2, and a C-terminal motif (Fig. 6). Both TPR-1 and the C terminus are involved in terminal protein interaction, while TPR-2 is required for the strand displacement activity and the high processivity of the DNA polymerase (24–26). PRD1 and phi29 DNA polymerases are primed by a terminal protein (TP) covalently attached to the ends of their linear genomes (27). Protein-primed DNA replication is employed by various biological entities containing a linear double-stranded genome. These include some bacterial and eukaryotic viruses, linear plasmids from bacteria, fungi, and plants (27, 28), transposable elements (29), and mitochondrial DNA (30). Related protein-primed DNA polymerases are also encoded by certain archaeal casposons (31). It has been suggested that a TP exists in these systems. In general, however, TPs are highly divergent and are not recognizably similar even between members of the same virus family (32). So far, only three other archaeal viruses, i.e.,

AQ:B/F6

zjv-jvi/zjv00518/zjv3323d18z | xppws | S=3 | 12/16/17 | 5:49 | 4/Color Fig: 2,4,5,6,9,10 | ArtID: 01727-17 | DOI:10.1128/JVI.01727-17 | CE: ysf

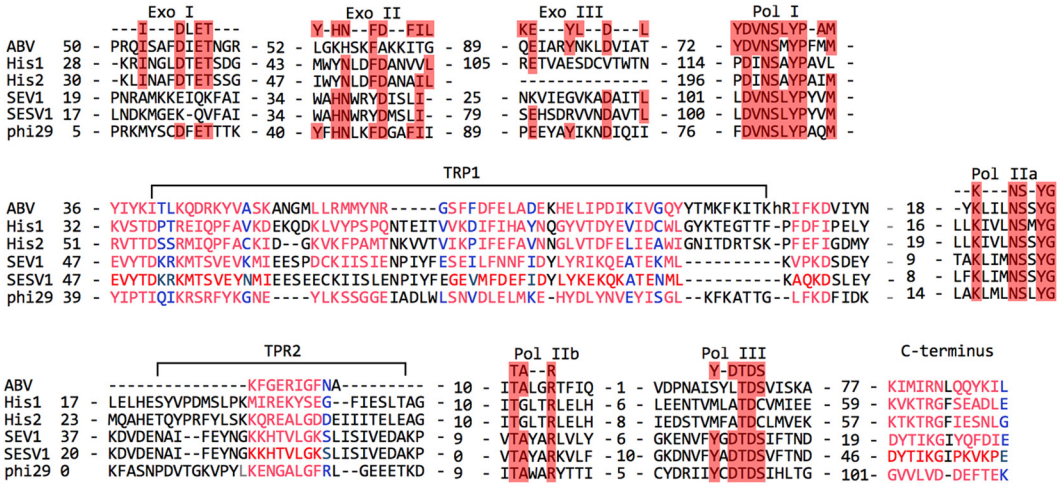

FIG 6 Sequence alignment of SEV1 ORF 665 and protein-primed DNA polymerases from bacteriophage phi29 and archaeal viruses ABV, His 1, and His2. Regions known to exist in protein-primed DNA polymerases (TPR-1, TPR-2, and C terminus) and the conserved motifs for the exonuclease activity (ExoI, -II, and -III) and the polymerization activity (Pol I, IIa, IIb, and III) are indicated. Numbers denote the numbers of amino acid residues between the motifs. Identical and similar bases are shown in red and orange, respectively.

Acidianus bottle-shaped virus (ABV) (33) and His1 and His2 (34), are known to encode a putative protein-primed DNA polymerase. The presence of a TP in these viruses was also suggested (33, 34) but was demonstrated only in His2 (35). No TP-encoding ORF was identified in the SEV1 genome by sequence searches. Therefore, the molecular mechanism of SEV1 DNA replication remains to be understood.

Virion composition. Analysis of the purified SEV1 virions by SDS-PAGE resolved four proteins, denoted VP1, VP2, VP3, and VP4, with estimated molecular masses of ~170, ~90, ~60, and ~12 kDa, respectively (Fig. 5B). Genes encoding these proteins (i.e., *vp1*, *vp2*, *vp3*, and *vp4*) were identified by mass spectrometry (Fig. 5A). The predicted molecular masses of the products of these genes are 50.2, 90.3, 72.3, and 11.8 kDa, respectively. All of them, except that for VP1, are in good agreement with the SDS-PAGE results. The predicted molecular mass of VP1 is considerably smaller than that estimated by SDS-PAGE, suggesting that the native VP1 protein might have undergone posttranslational modifications. VP4, the most abundant of the four proteins, appears to be the major capsid protein (MCP) of SEV1 and is presumably involved in the formation of the nucleoprotein filament. VP1 and VP2 are likely associated with the viral envelope since both of them possess transmembrane domains.

The virion shares several lipid species with the host cells, as revealed by mass spectrometry (Fig. 5C). These lipids include five compounds of isoprenoid glycerol dibiphytanyl glycerol tetraethers (GDGTs) (Fig. 5C) and isoprenoid diphytanyl glycerol diether (DGD, archaeol). GDGT4 was found to be the predominant GDGT compound, accounting for over one-half of the total core lipids, in both the host cell and the virion. Overall, the distribution pattern of the lipids in the virion envelope is similar, though nonidentical, to that of the host cell membrane. This observation contrasts sharply with those made on the filamentous virus Acidianus filamentous virus 1 (AFV1) (11) and the spindle-shaped virus SSV1 (36). A striking difference in lipid distribution between the virus envelopes of AFV1 or SSV1 and their respective host membranes exists. The most-predominant lipid species in the two viruses and in their hosts are GDGT-0 and GDGT-4, respectively. It is suggested that AFV1 and SSV1 selectively acquire GDGTs from the host membrane during progeny egress.

Infection of *Sulfolobus* sp. A20 by SEV1. Infection of *Sulfolobus* sp. A20 with SEV1 only slightly retarded the growth of the host cells (Fig. 7) and yielded no detectable cell debris (Fig. 8). To gain insight into the life cycle of SEV1, we monitored morphological changes of the virion and the host cell during the infection process by using several

zjv-jvi/zjv00518/zjv3323d18z | xppws | S=3 | 12/16/17 | 5:49 | 4/Color Fig: 2,4,5,6,9,10 | ArtID: 01727-17 | DOI:10.1128/JVI.01727-17 | CE: ysf

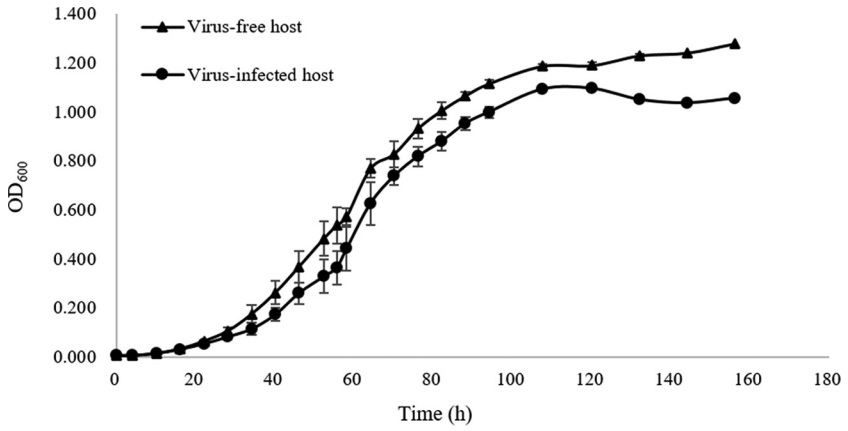

FIG 7 Influence of SEV1 infection on the growth of *Sulfolobus* sp. A20. Exponentially growing *Sulfolobus* sp. A20 cells were infected with SEV1. The infected cells were grown at 75°C in Zillig's medium. Samples were taken at indicated times, and the OD_{600} values of the samples were determined. Each data point represents an average of three independent measurements.

imaging techniques. An uninfected *Sulfolobus* sp. A20 cell was coccoid with irregular rises on the surface of the cell (Fig. 8A and B). Following SEV1 infection, clustered virions started to appear inside the host cell (Fig. 8C). Numerous granules of sizes similar to that of the SEV1 virion were also found in freeze-fractured infected cells (Fig. 8D). Coinciding with the appearance of virions, 6-fold pyramid-like protruding structures, known as virus-associated pyramids (VAPs) (17, 18), appeared at multiple sites on the cell surface (Fig. 8E and F). No VAPs were found on the surface of an uninfected cell. Ultrathin-sectioned cells infected by SEV1 were further analyzed by EM and 3-D ET (Fig. 9; see also Movie S3 in the supplemental material). We found that virion clusters in the cytoplasm of the infected cells were often close to VAPs, suggesting potential coupling between the formation of VAPs and the production of virions during SEV1 infection (Fig. 9). The electron density of the cytoplasm peripheral to the sites of virion assembly appeared more condensed than that in the rest of the cytoplasm (Fig. 8A and C and 9). Presumably, molecular machineries involved in processes such as viral DNA replication, transcription, translation, and assembly were enriched in the electron-dense region. Intriguingly, the existence of enveloped virions in the cytoplasm suggested that the virion acquired the lipid envelope inside the host cell (Fig. 8C and 9B and C). Rupture of a VAP led to the formation of a hexagonal opening on the cell surface, permitting the release of mature progeny virions (Fig. 8G and H). Multiple openings varying in size from 200 to 280 nm were seen on the surface of a single cell. These openings are all large enough for mature virions to move through. It is worth noting that the egress mechanism for SEV1 is consistent with the notion that the virion acquires the lipid envelope within the host cell. Ghost cells, which were left as empty shells after the release of virus particles and the host cell contents, remained in abundance in the culture even at a very late growth stage (Fig. 8I and J). This agrees well with the absence of cell debris and a decrease in cell density in the infected culture (Fig. 7).

DISCUSSION

Archaeal viruses represent a unique addition to the ever-expanding virosphere for their tremendous morphological and genomic diversity. In this report, we describe a novel archaeal virus, denoted SEV1, from an acidic hot spring in Costa Rica. The SEV1 virion has an ellipsoid shape never reported before in archaeal viruses. A 3-D ET analysis reveals an exceptional architecture for SEV1 virion. The virion capsid, enveloped by an 11-nm lipid membrane, displays 16 evenly spaced stripes and contains a cylindrical hole in the middle. The SEV1 capsid carries no protein shell and, instead, appears to be assembled from a nucleoprotein filament in a highly organized fashion (Fig. 10): the filament first wraps up around the longitudinal axis to form a multilayered flat disk-like

zjv-jvi/zjv00518/zjv3323d18z | xppws | S=3 | 12/16/17 | 5:49 | 4/Color Fig: 2,4,5,6,9,10 | ArtID: 01727-17 | DOI:10.1128/JVI.01727-17 | CE: ysf

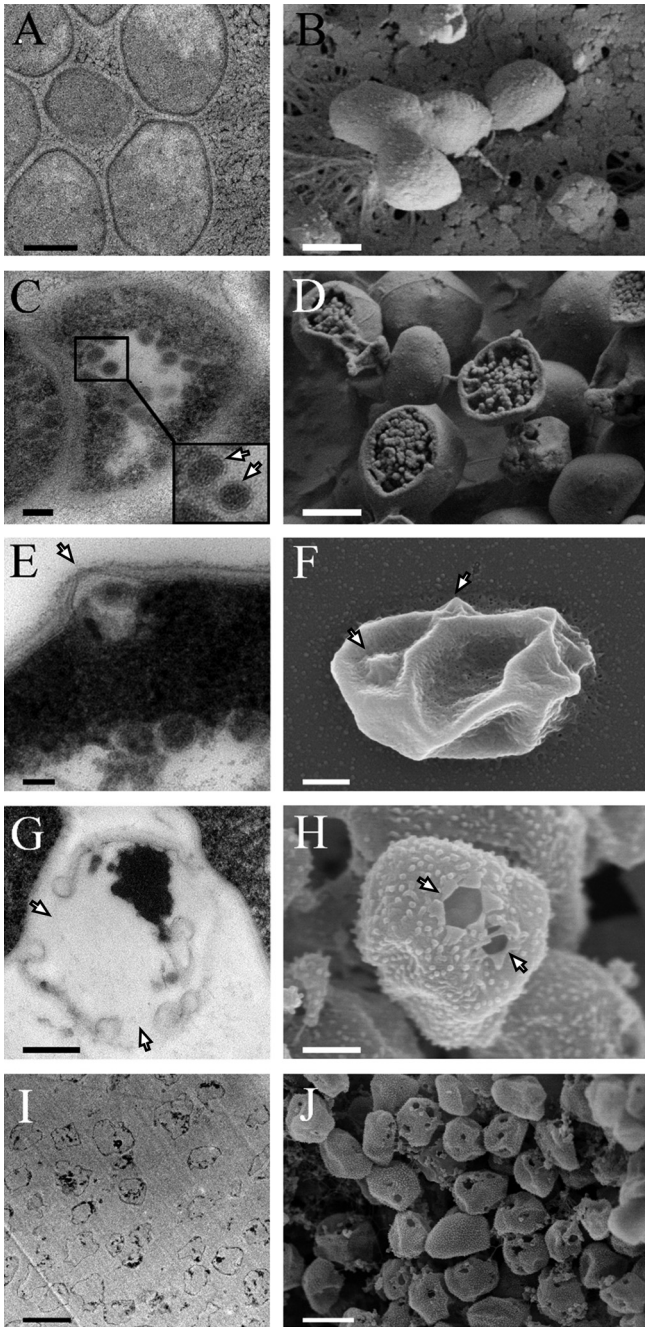

FIG 8 Analysis of the infection of *Sulfolobus* sp. A20 by SEV1 by TEM and SEM. (A and B) Virus-free host cells. (C and D) Assembly of virions in the infected host cells. The envelope of the virus particle is indicated by arrows. (E and F) Formation of VAPs on the cell surface. VAPs are indicated by arrows. (G and H) Hexagonal openings generated from VAPs on the cell surface. Arrows indicate where rupture of the VAPs occurred. (I and J) Empty ghost cells in the SEV1-infected culture at a late growth stage. Shown are TEM micrographs of the thin sections of infected cells (A, C, E, G, and I) and SEM micrographs of infected cells (B, D, F, H, and J). Bars: 500 nm (A), 1 μm (B), 100 nm (C), 1 μm (D), 50 nm (E), 200 nm (F), 200 nm (G), 200 nm (H), 2 μm (I), 1 μm (J).

structure and continue to extend to the next disk, and 16 of these structures then stack up to produce a spool-like capsid. Given its great abundance, VP4, the major capsid protein of SEV1, may serve to package genome DNA into the nucleoprotein filament. The length of the entire nucleoprotein filament is similar to that of the SEV1 genome. Assuming six layers per disk, the contour length of the filament in the capsid is estimated to be ~7.7 μm, a value close to the size of the viral genome (~7.9 μm).

zjv-jvi/zjv00518/zjv3323d18z | xppws | S=3 | 12/16/17 | 5:49 | 4/Color Fig: 2,4,5,6,9,10 | ArtID: 01727-17 | DOI:10.1128/JVI.01727-17 | CE: ysf

COLOR

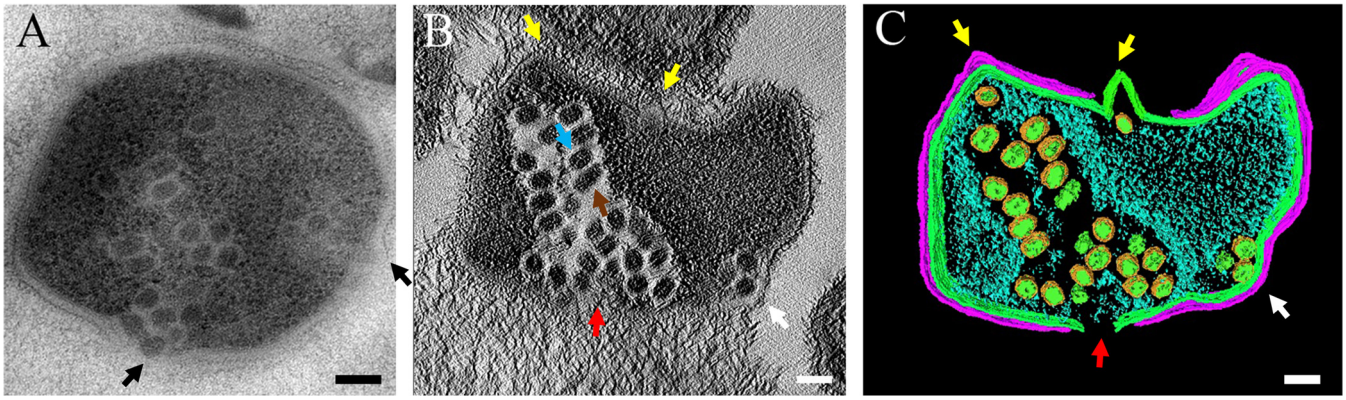

FIG 9 Assembly of SEV1 virions in the cytoplasm of the host cell. (A) TEM micrograph of the thin section of a SEV1-infected cell showing clusters of SEV1 virions in the cytoplasm of the host cell. Black arrows show VAPs on the cell surface, which are located in close proximity to clusters of SEV1 virions in the cytoplasm. (B) A single slice from the electron tomogram of an ultrathin-sectioned SEV1-infected host cell. (C) A segmented and surface-rendering display of the tomogram in panel B, showing various structures and components with different colors, including the S layer (purple), capsid (gray-green), cell membrane (green), virus envelope (orange), and cytoplasm (blue). A slight rise (white arrow), a VAP (yellow arrow), and a VAP opening (red arrow) on the surface of the infected cell are visible. Naked and enveloped virions are indicated by brown and blue arrows, respectively. Bar, 100 nm.

Compared to other viral genome packaging strategies, multilayered nucleoprotein wrapping, as employed by SEV1, allows viral DNA to be packaged more tightly while protected effectively by bound proteins. This unusual capsid architecture may represent a strategy for a virus to survive in a hot and acidic habitat. Interestingly, *Sulfolobus polyhedral virus 1* (SPV1), a recently reported hot spring virus, appears to have a thread ball-like capsid bearing resemblance in DNA packaging to that of SEV1 (13).

SEV1 infection resulted in no significant retardation in the growth of the host cell, producing no detectable cell debris. This observation agrees with the ability of the SEV1-infected cells to form colonies. However, the virus was capable of lysing the infected cells, generating ghost cells, as revealed by the TEM and scanning electron microscope (SEM) analyses of the SEV1-infected cells in the late stage of infection. Therefore, it appears that the rupture of the SEV1-infected cells is triggered under certain conditions. The release of mature virus particles involves the formation of a multitude of virus-associated pyramids on the surface of the infected cell. Notably, the intracellular space in which virion assembly occurs appears to be located close to the cell surface where a VAP is formed, indicating mechanistic coupling between the two processes. The opening of VAPs allows the release of mature virus particles. The mechanism of SEV1 release resembles that reported for the rod-shaped virus *Sulfolobus islandicus rod-shaped virus 2* (SIRV2) and the spherical virus *Sulfolobus turreted icosahedral virus* (STIV) (17, 18). However, SEV1 uses a hexagonal pyramidal structure, whereas SIRV2 and STIV employ a seven-sided pyramid. The hexagonal pyramids were also found on the surface of UV-irradiated *Pyrobaculum* cells, although viral replication could not be demonstrated (19). The difference between SEV1, SIRV2, and STIV in their

COLOR

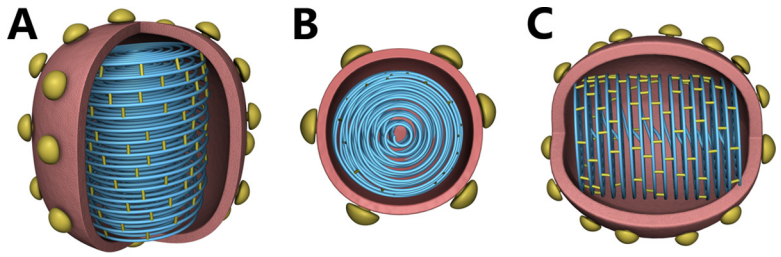

FIG 10 Schematic 3-D model of the SEV1 virion. (A) A nucleoprotein filament (blue) is coiled to form a disk, and 16 of these disks are stacked to form the capsid. Protein cross-links (yellow) exist between layers of the filament. The capsid is enveloped by a lipid membrane (brown) decorated with spikes (dark yellow). (B) Top view of the model. (C) Side view of the model.

pyramidal structures probably explains why no gene encoding a homologue of P98 (37–39) or C92 (40, 41), a protein capable of self-assembly into a VAP in SIRV2 or STIV, respectively, was readily identifiable through sequence comparison in the SEV1 genome. Taken together, our results support the notion that the VAP-based egress strategy is widely employed by *Sulfolobus* viruses of different morphologies, and, therefore, morphogenesis and virion release pathways are independently evolved in archaeal viruses.

Strikingly, as an enveloped virus, SEV1 acquires the lipid membrane within the cell. Electron micrographs of the thin sections of SEV1-infected cells clearly show that the enveloped viral capsids clustered in the cytoplasm, indicating that the SEV1 virion acquired the lipid membrane intracellularly. Therefore, SEV1 contrasts sharply with most enveloped viruses, which escape from host cells by budding, during which they obtain a lipid membrane enclosing the capsid (42). Very few enveloped viruses are known to acquire their lipid membrane inside the host cell (43). The vaccinia virus becomes enveloped through the use of membrane sheets derived from preexisting cellular membranes (44). Bacteriophage phi6 obtains its lipid membrane inside the host cell by membrane vesiculation or invagination (45). Acquisition of lipid membrane has not been extensively studied in the enveloped archaeal viruses. The *Sulfolobus* virus SSV1 was reported to obtain the lipid membrane through budding (16). STIV, a structurally unusual virus, possesses an icosahedral protein shell and an inner membrane enclosing a circular dsDNA genome (6). The viral membrane lipids are believed to be synthesized *de novo* (46). The insertion of the MCP into the lipid layer through its C terminus anchors the internal membrane to the protein shell. In comparison, the SEV1 virion was enveloped in the cytoplasm of the infected host cell, which lacks an inner membrane system, and released through VAPs. Therefore, it appears unlikely for the virus to acquire the membrane through either budding or membrane vesiculation. Lipid analysis shows that the SEV1 envelope contains a similar but nonidentical set of the host membrane lipids. Differences in lipid distribution between virions and host cells are also found in other archaeal viruses, i.e., STIV (47), SSV1 (36), and AFV1 (11). The lipid asymmetry probably results from a selective incorporation of lipids into the virion. These data suggest possible coordination between the virion and the host cell in membrane biogenesis. SEV1 appears to acquire lipids from a host lipid pool for the *de novo* assembly of its envelope.

MATERIALS AND METHODS

Enrichment cultures and virus-like particles. A sediment sample was collected from an acidic hot spring (pH 2.2 to 2.5, 86 to 106°C) in Lagura Fumarolica, Costa Rica (10°46′365″N, 85°20′646″W) and inoculated in Zillig's medium (20, 21). Incubation was carried out at 75°C with shaking at 150 rpm until growth was apparent (~9 days). The culture was filtered through a 0.45-μm polyvinylidene difluoride (PVDF) membrane (Merck Millipore). The cell-free supernatant was examined under EM for the presence of virus-like particles.

SEV1 and *Sulfolobus* sp. A20. The enrichment culture containing VLPs including SEV1 was plated on a Zillig's medium plate. Single colonies were picked and examined for the presence of VLPs by EM and PCR targeting SEV1 DNA. Cells from colonies devoid of any VLP were further purified by colony purification. A resulting strain susceptible to infection by SEV1 was designated as the host strain for SEV1. The strain was later shown to be a novel *Sulfolobus* species, denoted *Sulfolobus* sp. A20 (21). To purify SEV1, a growing culture of *Sulfolobus* sp. A20 was infected with the cell-free supernatant of the enrichment culture containing VLPs including SEV1. The culture was plated on a Zillig's medium plate, and colonies were picked. The colonies were examined for the presence of SEV1 by EM and PCR, and those containing SEV1 alone were further purified by repeated colony picking.

SEV1 virion preparation. *Sulfolobus* sp. A20 was grown in Zillig's medium at 75°C to an optical density at 600 nm (OD_{600}) of 0.4 to 0.6 and infected with a sample of SEV1. The infected culture was grown to an OD_{600} of 0.8 to 1.0 and centrifuged at 14,087 × *g* for 20 min at 4°C. The virus particles were collected from the cell-free supernatant by ultracentrifugation at 82,667 × *g* for 2 h at 4°C and resuspended in Zillig's basal salt. To purify the SEV1 virion, the concentrated SEV1 sample was subjected to CsCl gradient centrifugation (0.45 g/ml CsCl, 214,200 × *g* for 24 h at 4°C). The SEV1 particles for TEM observations were concentrated from the cell-free supernatant by ultrafiltration in an Amicon stirred cell (Merck Millipore).

Infection experiments. Exponentially growing *Sulfolobus* sp. A20 cells were harvested and mixed with SEV1 at a multiplicity of infection (MOI) of ~3. The infected cells were inoculated in Zillig's medium,

zjv-jvi/zjv00518/zjv3323d18z | xppws | S=3 | 12/16/17 | 5:49 | 4/Color Fig: 2,4,5,6,9,10 | ArtID: 01727-17 | DOI:10.1128/JVI.01727-17 | CE: ysf

and the culture was incubated at 75°C with shaking. Samples were taken at intervals, and the OD_{600} values of the samples were determined.

Viral DNA extraction. A sample of SEV1 was digested for 3 h at 50°C with proteinase K (0.8 mg/ml) in the presence of 1% SDS. Cetyltrimethylammonium bromide (CTAB) and NaCl were added to final concentrations of 1% and 0.8 M, respectively. After incubation for 10 min at 65°C, the sample was extracted with phenol-chloroform, and the viral DNA was precipitated with ethanol.

DNA sequencing and genome analysis. The genomic DNA of SEV1 was digested with EcoRI, EcoRV, KpnI, or BamHI, separately. The restriction fragments were gel purified (Wizard SV Gel and PCR Cleanup System; Promega) and ligated with linear pUC18 plasmid digested with a corresponding restriction enzyme. Ligation products were transformed into *Escherichia coli* TransT1 strains (TransGen Biotech). Plasmids from the transformed cells were isolated, and inserts in the plasmids were sequenced. Sequences were assembled with VectorNTI, and sequence gaps were filled by PCR. The terminal sequences of the viral genome were determined by primer walking using Sanger's method with viral DNA as the template and a primer directing synthesis toward either end of the genome from outside the corresponding inverted terminal repeat. Base calling was done by BioEdit. Gene prediction was carried out using ORFfinder (https://www.ncbi.nlm.nih.gov/orffinder/). Sequence comparison and secondary structure prediction were performed with BLASTP (https://blast.ncbi.nlm.nih.gov/Blast.cgi) and SMART (http://smart.embl-heidelberg.de/), respectively.

AQ: C

Analysis of virion proteins. A sample of SEV1, purified by CsCl gradient ultracentrifugation, was loaded onto a 15% SDS-PAGE gel. The gel was stained with Coomassie brilliant blue G250. Proteins were recovered from the stained gel and identified by liquid chromatography-tandem mass spectrometry (LC-MS/MS).

Lipid analysis. Total lipids were extracted as described previously with modifications (48, 49). A mixture of methanol (MeOH)-dichloromethane (DCM)-phosphate buffer (PB) (2:1:0.8 by volume) was added to the sample. After sonication, the ratio of MeOH to DCM to PB was adjusted to 1:1:0.9. Following phase separation, the organic phase was collected. The process of solvent extraction was repeated twice, and the extracts were combined. After the addition of internal standards (C46, 10 μl), the sample was dried, and GDGTs were detected by high-pressure liquid chromatography (HPLC)-MS as described previously (50).

AQ: D

Negative-stain transmission electron microscopy. For negative-stain TEM, purified SEV1 virions were stained with 2% (wt/vol) uranyl acetate and observed under a JEM-1400 (JEOL) TEM (51).

Cryo-electron microscopy and cryo-electron tomography. A sample (~3.5 μl) of purified SEV1 virions was deposited on a 200-mesh quantifoil R2/1 copper EM grid coated with a thin holey carbon film. After blotting excess solution with a filter paper, the grid was rapidly plunged into liquid ethane, transferred into a liquid-nitrogen-cooled side entry Gatan 626 cryo holder, and inserted into an FEI Talos F20C cryo-electron microscope equipped with a field emission gun and operated at an acceleration voltage of 200 kV for observation. EM micrographs were taken at a magnification of ×22,000 in a direct-electron-detecting camera (DE-20; Direct Electron Co.) in correspondence to 2.02 Å/pixel. For cryo-ET analysis, tilt series images were collected using the serialEM software package (52) with a tilt range from −60° to 60° in increments of 2° at a magnification of ×22,000. The collected tilt series were processed, and 3-D tomographic reconstructions of SEV1 virions were performed using the IMOD (53) and ICON software packages (54). The ET volumes were segmented, surface rendered, and displayed in 3-D with Amira software (FEI Visualization Sciences Group).

ET of negatively stained virions. A sample of purified SEV1 virions was negatively stained with 2% uranyl acetate and applied to a carbon-coated specimen grid. The excess liquid was blotted away, and the dried grid was inserted into an FEI Tecnai electron microscope operated at an acceleration voltage of 200 kV. EM micrographs were taken at a magnification of ×50,000 by a charge-coupled-device (CCD) camera (Gatan US1000 894) with 2.21 Å/pixel. Tilt-series images were collected using the serialEM software package (52) and processed by the Protomo software package (55). The volume segmentations were carried out with the Amira software (FEI Visualization Sciences Group).

Ultrathin section of SEV1-infected cells. SEV1-infected cells were drawn into a carrier and quickly frozen in a Leica EM HPM100 high-pressure freezer. The frozen samples were subjected to a substitution process in Leica EM AFS2 with a 2% osmium tetroxide-acetone solution and then infiltrated sequentially with 25%, 50%, and 75% Spurr-acetone for 3 h in each solution. The samples were then embedded in 100% Spurr resin and polymerized at 45°C for 12 h and 60°C for 24 h. The samples in the embedding block were cut into 70-nm-thick ultrathin sections by a diamond knife on a Leica UC6 ultramicrotome, stained with 2% uranyl acetate and 0.1% lead citrate, and observed in an FEI Sprit electron microscope operated at 120 kV.

Electron tomography of SEV1-infected cells. The ultrathin sections of SEV1-infected cells were put into a Tecnai Spirit, operated at 120 kV (FEI), and subjected to an ET analysis. The tilt series were collected using the SerialEM software package (53) on an Eagle CCD (FEI) camera at a magnification of ×30,000 in correspondence to 7.54 Å/pixel, with a total dose of ~120 $e^-/Å^2$. The tilt angles ranged from around −45° to 45° at 2-degree increments. The collected tilt series images were processed, and the 3-D electron tomograms were reconstructed using the software package Protomo, version 2.2.1 (55). The ET volumes were segmented, surface rendered, and displayed in 3-D with Amira software (FEI Visualization Sciences Group).

Scanning electron microscopy. SEV1-infected cells were fixed in 2.5% glutaraldehyde for 12 h at 4°C, washed with Zillig's basal salt for three times, dehydrated through a graded series of ethanol dilutions, and critical-point dried (Bal-Tec CPD 030). The dried coverslips were sputtered with 5- to 8-nm

zjv-jvi/zjv00518/zjv3323d18z | xppws | S=3 | 12/16/17 | 5:49 | 4/Color Fig: 2,4,5,6,9,10 | ArtID: 01727-17 | DOI:10.1128/JVI.01727-17 | CE: ysf

platinum, and the samples were observed under a field emission scanning electron microscope (Hitachi SU8010).

Freeze fracture and cryo-SEM. SEV1 virions were loaded onto a specimen shutter, frozen in liquid nitrogen, and transferred into a cryo-SEM preparation chamber. Freeze fracture was carried out by using the micrometer-advanced rigid blade. Autosublimation was performed for 20 min at −90°C in a cryo-SEM work station (Quorum PP3010T). The specimen was observed under a field emission scanning electron microscope (Hitachi SU8010).

AQ: E **Availability of data.** The SEV1 genome sequence has been deposited in GenBank under accession number MF144115.

SUPPLEMENTAL MATERIAL

Supplemental material for this article may be found at https://doi.org/10.1128/JVI.01727-17.

SUPPLEMENTAL FILE 1, MP4 file, 1.2 MB.
SUPPLEMENTAL FILE 2, MP4 file, 3.9 MB.
SUPPLEMENTAL FILE 3, MP4 file, 5.0 MB.
SUPPLEMENTAL FILE 4, PDF file, 0.1 MB.
SUPPLEMENTAL FILE 5, PDF file, 0.1 MB.

ACKNOWLEDGMENTS

Our electron microscopy-related work, including negatively staining EM, cryo-EM, and electron tomography, was performed at the Center for Biological Imaging (CBI), Institute of Biophysics, Chinese Academy of Sciences. We are grateful to X. Huang, G. Ji, Z. Guo, B. Zhu, W. Ding, D. Fan, T. Niu, F. Sun, and other staff members at CBI for their excellent technical support in cryo-EM and ET data collection and HPC-service station. We also thank J. Liang and C. Li for assistance with the use of TEM and SEM in the Institute of Microbiology, Chinese Academy of Sciences.

This work was supported by National Natural Science Foundation of China (NSFC) grants 31130003, 31730001, and 30730003 to L.H. and NSFC grants 31425007 and 31230018 to P.Z.

REFERENCES

1. Wang H, Peng N, Shah SA, Huang L, She Q. 2015. Archaeal extrachromosomal genetic elements. Microbiol Mol Biol Rev 79:117–152. https://doi.org/10.1128/MMBR.00042-14.
2. Prangishvili D. 2013. The wonderful world of archaeal viruses, p 565–585. Annu Rev Microbiol 67:565–585. https://doi.org/10.1146/annurev-micro-092412-155633.
3. Adams MJ, Lefkowitz EJ, King AMQ, Harrach B, Harrison RL, Knowles NJ, Kropinski AM, Krupovic M, Kuhn JH, Mushegian AR, Nibert M, Sabanadzovic S, Sanfacon H, Siddell SG, Simmonds P, Varsani A, Zerbini FM, Gorbalenya AE, Davison AJ. 2017. Changes to taxonomy and the International Code of Virus Classification and Nomenclature ratified by the International Committee on Taxonomy of Viruses. Arch Virol 162:2505–2538. https://doi.org/10.1007/s00705-017-3358-5.
4. Snyder JC, Bolduc B, Young MJ. 2015. 40 Years of archaeal virology: expanding viral diversity. Virology 479:369–378. https://doi.org/10.1016/j.virol.2015.03.031.
5. Prangishvili D, Bamford DH, Forterre P, Iranzo J, Koonin EV, Krupovic M. 2017. The enigmatic archaeal virosphere. Nat Rev Microbiol 15:724–739. https://doi.org/10.1038/nrmicro.2017.125.
6. Rice G, Tang L, Stedman K, Roberto F, Spuhler J, Gillitzer E, Johnson JE, Douglas T, Young M. 2004. The structure of a thermophilic archaeal virus shows a double-stranded DNA viral capsid type that spans all domains of life. Proc Natl Acad Sci U S A 101:7716–7720. https://doi.org/10.1073/pnas.0401773101.
7. Porter K, Kukkaro P, Bamford JK, Bath C, Kivela HM, Dyall-Smith ML, Bamford DH. 2005. SH1: a novel, spherical halovirus isolated from an Australian hypersaline lake. Virology 335:22–33. https://doi.org/10.1016/j.virol.2005.01.043.
8. Rensen EI, Mochizuki T, Quemin E, Schouten S, Krupovic M, Prangishvili D. 2016. A virus of hyperthermophilic archaea with a unique architecture among DNA viruses. Proc Natl Acad Sci U S A 113:2478–2483. https://doi.org/10.1073/pnas.1518929113.
9. Stedman KM, DeYoung M, Saha M, Sherman MB, Morais MC. 2015. Structural insights into the architecture of the hyperthermophilic Fusellovirus SSV1. Virology 474:105–109. https://doi.org/10.1016/j.virol.2014.10.014.
10. DiMaio F, Yu X, Rensen E, Krupovic M, Prangishvili D, Egelman EH. 2015. A virus that infects a hyperthermophile encapsidates A-form DNA. Science 348:914–917. https://doi.org/10.1126/science.aaa4181.
11. Pet E, DiMaio F, Yu X, Lucas-Staat S, Krupovic M, Schouten S, Prangishvili D, Egelman EH. 2017. Model for a novel membrane envelope in a filamentous hyperthermophilic virus. Elife 6:e26268. https://doi.org/10.7554/eLife.26268.
12. Haring M, Peng X, Brugger K, Rachel R, Stetter KO, Garrett RA, Prangishvili D. 2004. Morphology and genome organization of the virus PSV of the hyperthermophilic archaeal genera *Pyrobaculum* and *Thermoproteus*: a novel virus family, the Globuloviridae. Virology 323:233–242. https://doi.org/10.1016/j.virol.2004.03.002.
13. Liu Y, Ishino S, Ishino Y, Pehau-Arnaudet G, Krupovic M, Prangishvili D. 2017. A novel type of polyhedral viruses infecting hyperthermophilic archaea. J Virol 91:e00589-17. https://doi.org/10.1128/JVI.00589-17.
14. Haring M, Rachel R, Peng X, Garrett RA, Prangishvili D. 2005. Viral diversity in hot springs of Pozzuoli, Italy, and characterization of a unique archaeal virus, acidianus bottle-shaped virus, from a new family, the Ampullaviridae. J Virol 79:9904–9911. https://doi.org/10.1128/JVI.79.15.9904-9911.2005.
15. Mochizuki T, Krupovic M, Pehau-Arnaudet G, Sako Y, Forterre P, Prangishvili D. 2012. Archaeal virus with exceptional virion architecture and the largest single-stranded DNA genome. Proc Natl Acad Sci U S A 109:13386–13391. https://doi.org/10.1073/pnas.1203668109.
16. Quemin ERJ, Chlanda P, Sachse M, Forterre P, Prangishvili D, Krupovic M. 2016. Eukaryotic-like virus budding in archaea. mBio 7(5):e01439-16. https://doi.org/10.1128/mBio.01439-16.
17. Bize A, Karlsson EA, Ekefjard K, Quax TEF, Pina M, Prevost MC, Forterre P, Tenaillon O, Bernander R, Prangishvili D. 2009. A unique virus release

zjv-jvi/zjv00518/zjv3323d18z | xppws | S=3 | 12/16/17 | 5:49 | 4/Color Fig: 2,4,5,6,9,10 | ArtID: 01727-17 | DOI:10.1128/JVI.01727-17 | CE: ysf

mechanism in the Archaea. Proc Natl Acad Sci U S A 106:11306–11311. https://doi.org/10.1073/pnas.0901238106.
18. Brumfield SK, Ortmann AC, Ruigrok V, Suci P, Douglas T, Young MJ. 2009. Particle assembly and ultrastructural features associated with replication of the lytic archaeal virus *Sulfolobus* turreted icosahedral virus. J Virol 83:5964–5970. https://doi.org/10.1128/JVI.02668-08.
19. Rensen E, Krupovic M, Prangishvili D. 2015. Mysterious hexagonal pyramids on the surface of Pyrobaculum cells. Biochimie 118:365–367. https://doi.org/10.1016/j.biochi.2015.06.007.
20. Zillig W, Kletzin A, Schleper C, Holz I, Janekovic D, Hain J, Lanzendorfer M, Kristjansson JK. 1994. Screening for Sulfolobales, their plasmids and their viruses in Icelandic solfataras. Syst Appl Microbiol 16:609–628. https://doi.org/10.1016/S0723-2020(11)80333-4.
21. Dai X, Wang H, Zhang Z, Li K, Zhang X, Mora-López M, Jiang C, Liu C, Wang L, Zhu Y, Hernández-Ascencio W, Dong Z, Huang L. 2016. Genome sequencing of *Sulfolobus* sp A20 from Costa Rica and comparative analyses of the putative pathways of carbon, nitrogen, and sulfur metabolism in various *Sulfolobus* strains. Front Microbiol 7:1902. https://doi.org/10.3389/fmicb.2016.01902.
22. Savilahti H, Caldentey J, Lundström K, Syväoja JE, Bamford DH. 1991. Overexpression, purification, and characterization of *Escherichia coli* bacteriophage PRD1 DNA polymerase. *In vitro* synthesis of full-length PRD1 DNA with purified proteins. J Biol Chem 266:18737–18744.
23. Blanco L, Salas M. 1996. Relating structure to function in phi29 DNA polymerase. J Biol Chem 271:8509–8512. https://doi.org/10.1074/jbc.271.15.8509.
24. Dufour E, Mendez J, Lazaro JM, de Vega M, Blanco L, Salas M. 2000. An aspartic acid residue in TPR-1, a specific region of protein-priming DNA polymerases, is required for the functional interaction with primer terminal protein. J Mol Biol 304:289–300. https://doi.org/10.1006/jmbi.2000.4216.
25. Truniger V, Lázaro JM, Salas M. 2004. Function of the C-terminus of phi29 DNA polymerase in DNA and terminal protein binding. Nucleic Acids Res 32:361–370. https://doi.org/10.1093/nar/gkh184.
26. Rodríguez I, Lázaro JM, Blanco L, Kamtekar S, Berman AJ, Wang J, Steitz TA, Salas M, de Vega M. 2005. A specific subdomain in phi 29 DNA polymerase confers both processivity and strand-displacement capacity. Proc Natl Acad Sci U S A 102:6407–6412. https://doi.org/10.1073/pnas.0500597102.
27. Salas M. 1991. Protein-priming of DNA-replication. Annu Rev Biochem 60:39–71. https://doi.org/10.1146/annurev.bi.60.070191.000351.
28. Meinhardt F, Schaffrath R, Larsen M. 1997. Microbial linear plasmids. Appl Microbiol Biotechnol 47:329–336. https://doi.org/10.1007/s002530050936.
29. Kapitonov VV, Jurka J. 2006. Self-synthesizing DNA transposons in eukaryotes. Proc Natl Acad Sci U S A 103:4540–4545. https://doi.org/10.1073/pnas.0600833103.
30. Fricova D, Valach M, Farkas Z, Pfeiffer I, Kucsera J, Tomaska L, Nosek J. 2010. The mitochondrial genome of the pathogenic yeast *Candida subhashii*: GC-rich linear DNA with a protein covalently attached to the 5′ termini. Microbiology 156:2153–2163. https://doi.org/10.1099/mic.0.038646-0.
31. Krupovic M, Beguin P, Koonin EV. 2017. Casposons: mobile genetic elements that gave rise to the CRISPR-Cas adaptation machinery. Curr Opin Microbiol 38:36–43. https://doi.org/10.1016/j.mib.2017.04.004.
32. Redrejo-Rodriguez M, Munoz-Espin D, Holguera I, Mencia M, Salas M. 2012. Functional eukaryotic nuclear localization signals are widespread in terminal proteins of bacteriophages. Proc Natl Acad Sci U S A 109:18482–18487. https://doi.org/10.1073/pnas.1216635109.
33. Peng X, Basta T, Haring M, Garrett RA, Prangishvili D. 2007. Genome of the *Acidianus* bottle-shaped virus and insights into the replication and packaging mechanisms. Virology 364:237–243. https://doi.org/10.1016/j.virol.2007.03.005.
34. Bath C, Cukalac T, Porter K, Dyall-Smith ML. 2006. His1 and His2 are distantly related, spindle-shaped haloviruses belonging to the novel virus group, *Salterprovirus*. Virology 350:228–239. https://doi.org/10.1016/j.virol.2006.02.005.
35. Porter K, Dyall-Smith ML. 2008. Transfection of haloarchaea by the DNAs of spindle and round haloviruses and the use of transposon mutagenesis to identify non-essential regions. Mol Microbiol 70:1236–1245. https://doi.org/10.1111/j.1365-2958.2008.06478.x.
36. Quemin ERJ, Pietila MK, Oksanen HM, Forterre P, Rijpstra WIC, Schouten S, Bamford DH, Prangishvili D, Krupovic M. 2015. *Sulfolobus* spindle-shaped virus 1 contains glycosylated capsid proteins, a cellular chromatin protein, and host-derived lipids. J Virol 89:11681–11691. https://doi.org/10.1128/JVI.02270-15.
37. Quax TEF, Krupovic M, Lucas S, Forterre P, Prangishvili D. 2010. The *Sulfolobus* rod-shaped virus 2 encodes a prominent structural component of the unique virion release system in Archaea. Virology 404:1–4. https://doi.org/10.1016/j.virol.2010.04.020.
38. Quax TEF, Lucas S, Reimann J, Pehau-Arnaudet G, Prevost MC, Forterre P, Albers SV, Prangishvili D. 2011. Simple and elegant design of a virion egress structure in Archaea. Proc Natl Acad Sci U S A 108:3354–3359. https://doi.org/10.1073/pnas.1018052108.
39. Daum B, Quax TEF, Sachse M, Mills DJ, Reimann J, Yildiz Ö, Häder S, Saveanu C, Forterre P, Albers S-V, Kühlbrandt W, Prangishvili D. 2014. Self-assembly of the general membrane-remodeling protein PVAP into sevenfold virus-associated pyramids. Proc Natl Acad Sci U S A 111:3829–3834. https://doi.org/10.1073/pnas.1319245111.
40. Snyder JC, Brumfield SK, Peng N, She QX, Young MJ. 2011. *Sulfolobus* turreted icosahedral virus c92 protein responsible for the formation of pyramid-like cellular lysis structures. J Virol 85:6287–6292. https://doi.org/10.1128/JVI.00379-11.
41. Snyder JC, Brumfield SK, Kerchner KM, Quax TEF, Prangishvili D, Young MJ. 2013. Insights into a viral lytic pathway from an archaeal virus-host system. J Virol 87:2186–2192. https://doi.org/10.1128/JVI.02956-12.
42. Garoff H, Hewson R, Opstelten D-JE. 1998. Virus maturation by budding. Microbiol Mol Biol Rev 62:1171–1190.
43. Bamford DH, Palva ET, Lounatmaa K. 1976. Ultrastructure and life-cycle of lipid-containing bacteriophage-phi6. J Gen Virol 32:249–259. https://doi.org/10.1099/0022-1317-32-2-249.
44. Chlanda P, Carbajal MA, Cyrklaff M, Griffiths G, Krijnse-Locker J. 2009. Membrane rupture generates single open membrane sheets during vaccinia virus assembly. Cell Host Microbe 6:81–90. https://doi.org/10.1016/j.chom.2009.05.021.
45. Laurinavičius S, Käkeläa R, Bamford DH, Somerharju P. 2004. The origin of phospholipids of the enveloped bacteriophage phi6. Virology 326:182–190. https://doi.org/10.1016/j.virol.2004.05.021.
46. Fu C-Y, Wang K, Gan L, Lanman J, Khayat R, Young MJ, Jensen GJ, Doerschuk PC, Johnson JE. 2010. *In vivo* assembly of an archaeal virus studied with whole-cell electron cryotomography. Structure 18:1579–1586. https://doi.org/10.1016/j.str.2010.10.005.
47. Maaty WSA, Ortmann AC, Dlakic M, Schulstad K, Hilmer JK, Liepold L, Weidenheft B, Khayat R, Douglas T, Young MJ, Bothner B. 2006. Characterization of the archaeal thermophile Sulfolobus turreted icosahedral virus validates an evolutionary link among double-stranded DNA viruses from all domains of life. J Virol 80:7625–7635. https://doi.org/10.1128/JVI.00522-06.
48. Bligh EG, Dyer WJ. 1959. A rapid method of total lipid extraction and purification. Can J Biochem Physiol 37:911–917.
49. Pitcher A, Hopmans EC, Mosier AC, Park S-J, Rhee S-K, Francis CA, Schouten S, Damsté JSS. 2011. Core and intact polar glycerol dibiphytanyl glycerol tetraether lipids of ammonia-oxidizing archaea enriched from marine and estuarine sediments. Appl Environ Microbiol 77:3468–3477. https://doi.org/10.1128/AEM.02758-10.
50. Zhang CL, Wang J, Wei Y, Zhu C, Huang L, Dong H. 2012. Production of branched tetraether lipids in the lower Pearl River and estuary: effects of extraction methods and impact on bGDGT proxies. Front Microbiol 2:274. https://doi.org/10.3389/fmicb.2011.00274.
51. Xiang X, Chen L, Huang X, Luo Y, She Q, Huang L. 2005. *Sulfolobus tengchongensis* spindle-shaped virus STSV1: virus-host interactions and genomic features. J Virol 79:8677–8686. https://doi.org/10.1128/JVI.79.14.8677-8686.2005.
52. Mastronarde DN. 2005. Automated electron microscope tomography using robust prediction of specimen movements. J Struct Biol 152:36–51. https://doi.org/10.1016/j.jsb.2005.07.007.
53. Kremer JR, Mastronarde DN, McIntosh JR. 1996. Computer visualization of three-dimensional image data using IMOD. J Struct Biol 116:71–76. https://doi.org/10.1006/jsbi.1996.0013.
54. Deng Y, Chen Y, Zhang Y, Wang S, Zhang F, Sun F. 2016. ICON: 3D reconstruction with 'missing-information' restoration in biological electron tomography. J Struct Biol 195:100–112. https://doi.org/10.1016/j.jsb.2016.04.004.
55. Winkler H, Taylor KA. 2013. Marker-free dual-axis tilt series alignment. J Struct Biol 182:117–124. https://doi.org/10.1016/j.jsb.2013.02.004.

AUTHOR QUERIES

AUTHOR PLEASE ANSWER ALL QUERIES 1

AQau—Please confirm the given-names and surnames are identified properly by the colors. = Given-Name, = Surname

AQau—An ORCID ID was provided for at least one author during submission. Please click the name associated with the ORCID ID icon () in the byline to verify that the link is working and that it links to the correct author.

AQfund—The table below includes funding information that you provided on the submission form when you submitted the manuscript. This funding information will not appear in the article, but it will be provided to CrossRef and made publicly available. Please check it carefully for accuracy and mark any necessary corrections. If you would like statements acknowledging financial support to be published in the article itself, please make sure that they appear in the Acknowledgments section. Statements in Acknowledgments will have no bearing on funding data deposited with CrossRef and vice versa.

Funder	Grant(s)	Author(s)	Funder ID
National Natural Science Foundation of China (NSFC)	31130003, 31730001, 30730003	Li Huang	https://doi.org/10.13039/501100001809
National Natural Science Foundation of China (NSFC)	31425007, 31230018	Ping Zhu	https://doi.org/10.13039/501100001809

AQA—Please verify city for affiliation d.

AQB—Okay to change “TRP-1” and “TRP-2” to “TPR-1” and “TPR-2,” respectively, in “protein-primed DNA polymerases, i.e., TRP-1, TRP-2” (to match “TPR-1” and “TPR-2,” which occur later)? If not, please correct as necessary throughout.

AQC—Per ASM style, accession numbers for newly submitted sequences are given in a separate paragraph at the end of the text. Please check the new paragraph and verify the database.

AQD—If “performance” is better than “pressure” for the definition of HPLC, please correct.

AQE—ASM policy requires that sequence/protein/microarray data be available to the public upon online posting of the article, so please verify the accuracy of accession numbers for such data (particularly for new sequences) and that each number retrieves the full record of the data when used in a search in the database (not just the home page). Please also verify the database link, if included (hotlinks can be added only to GenBank, PDB, DDBJ, GEO, ArrayExpress, and BioSample/BioProject accession numbers). If the accession number is for a database that cannot be linked, please add the database name to the text. If the accession

AUTHOR QUERIES

AUTHOR PLEASE ANSWER ALL QUERIES 2

numbers for new data are not publicly accessible by the proof stage, publication of your article may be delayed; please contact the ASM production editor immediately with the expected release date.

AQF—The legend for Fig. 2B in the original pdf mentioned black arrows: "(B) Cryo-ET of SEV1 virions. The virus envelope, spikes on the envelope, and striated capsid are indicated by black, orange, and blue arrows, respectively"; however, there are no black arrows in Fig. 2B; if edits to this sentence are not correct, please make appropriate changes to the figure legend; if the figure needs to be changed, please upload a corrected figure (with corresponding changes in the legend, if necessary) with your proofs. Also, in the original pdf there was a description of a panel F for Fig. 2: "(F) A schematic 3-D model of the SEV1 virion. A nucleoprotein filament (blue) is coiled to form a disk, and 16 of these disks are stacked to form the capsid. Protein cross-links (yellow) exist between layers of the filament. The capsid is enveloped by a lipid membrane (brown) decorated with spikes (dark yellow)"; however, Fig. 2 has panels A to E only, and this description seems to be similar to that of Fig. 10; therefore, this portion of Fig. 2 legend has been deleted.